Globally significant greenhouse-gas emissions from African inland waters

Alberto V. Borges[1]*, François Darchambeau[1], Cristian R. Teodoru[2], Trent R. Marwick[2], Fredrick Tamooh[2,3], Naomi Geeraert[2], Fredrick O. Omengo[2], Frédéric Guérin[4], Thibault Lambert[1], Cédric Morana[2], Eric Okuku[2,5] and Steven Bouillon[2]

Carbon dioxide emissions to the atmosphere from inland waters—streams, rivers, lakes and reservoirs—are nearly equivalent to ocean and land sinks globally. Inland waters can be an important source of methane and nitrous oxide emissions as well, but emissions are poorly quantified, especially in Africa. Here we report dissolved carbon dioxide, methane and nitrous oxide concentrations from 12 rivers in sub-Saharan Africa, including seasonally resolved sampling at 39 sites, acquired between 2006 and 2014. Fluxes were calculated from published gas transfer velocities, and upscaled to the area of all sub-Saharan African rivers using available spatial data sets. Carbon dioxide-equivalent emissions from river channels alone were about 0.4 Pg carbon per year, equivalent to two-thirds of the overall net carbon land sink previously reported for Africa. Including emissions from wetlands of the Congo river increases the total carbon dioxide-equivalent greenhouse-gas emissions to about 0.9 Pg carbon per year, equivalent to about one quarter of the global ocean and terrestrial combined carbon sink. Riverine carbon dioxide and methane emissions increase with wetland extent and upland biomass. We therefore suggest that future changes in wetland and upland cover could strongly affect greenhouse-gas emissions from African inland waters.

Climate predictions necessitate a full and robust account of natural and anthropogenic greenhouse-gas (GHG) fluxes, especially for CO_2 (refs 1–3), CH_4 (ref. 4) and N_2O (ref. 5), which together accounted for 94% of the anthropogenic global radiative forcing by well-mixed GHGs in 2011 relative to 1750 (ref. 6). Inland waters (streams, rivers, lakes and reservoirs) are increasingly recognized as important sources of GHGs to the atmosphere, with global CO_2 and CH_4 emissions estimated at 2.1 PgC yr^{-1} (ref. 3) and 0.7 PgC yr^{-1} (CO_2-equivalents; CO_2e) (ref. 4) (1 Pg = 10^{15} g), respectively. Considering that the oceanic and land carbon (C) sinks correspond to ~1.5 and ~2.0 PgC yr^{-1} (ref. 7), respectively, the GHG flux from inland waters is significant in the global C budget.

In a recent global compilation of inland CO_2 data[3], <20 data points (out of 6,708, that is, <0.3%) represented African inland waters (with the exception of South Africa, which has been densely sampled), even though they account for ~12% of both global freshwater discharge[8] and riverine surface area[3], and include some of the largest rivers and lakes in the world. Equally for the global CH_4 database, there is a strong under-representation of tropical inland waters, whereby a recent synthesis[4] resorted to extrapolating CH_4 fluxes from temperate rivers.

The prevailing large uncertainty involved in GHG flux estimates for inland waters, essentially due to the paucity of available data, is coupled to a poor understanding of underlying processes, both of which preclude gauging of future fluxes in response to human pressures. In particular, there is a need to further understand the link between inland water GHG fluxes and catchment characteristics, in particular regarding their connectivity with upland terrestrial[9,10]

and wetland[11–13] C production and stocks. The CO_2 emissions from inland waters have been traditionally interpreted as fuelled by organic C from upland terrestrial biomass[1,14]. In the Amazon basin, CO_2 emissions from floodplain lakes[11] and from river channels[12,13] have been attributed to organic and inorganic C from wetlands (flooded forest and macrophytes). Finally, recently recognized biases in computed CO_2 data traditionally used in inland water studies[15,16] highlight the requirement for careful data-quality checking and future emphasis on high-quality direct CO_2 measurements.

In this study, we report an extensive compilation of dissolved CO_2, CH_4 and N_2O concentrations (Supplementary Table 1) gathered in 12 river basins in sub-Saharan Africa (SSA; Fig. 1 and Supplementary Fig. 1). The rivers range from 7.8×10^3 to 3.7×10^6 km^2 in watershed area and from 1.9 to 1.3×10^3 km^3 yr^{-1} in discharge, including the largest in Africa (Supplementary Table 2). A wide size range was sampled, from <1 m width (headwaters) to ~10 km width (mainstem Congo).

Variability of GHG concentrations and fluxes

The partial pressure of CO_2 (p_{CO_2}) values spanned two orders of magnitude, ranging between 300 and 16,942 ppm, CH_4 concentrations varied over five orders of magnitude, ranging between 2 and 62,966 nmol l^{-1}, whereas N_2O spanned three orders of magnitude, ranging between 0.2 and 85.4 nmol l^{-1} (Supplementary Fig. 2). The Congo River was the most variable in GHG concentrations, with distinct differences between streams (<100 m width) and rivers (>100 m width): p_{CO_2} and CH_4 values were higher in streams than rivers, whereas the opposite was observed for N_2O and oxygen saturation level

[1]Université de Liège, Unité d'Océanographie Chimique, Institut de Physique (B5), B-4000, Belgium. [2]Katholieke Universiteit Leuven, Department of Earth and Environmental Sciences, Celestijnenlaan 200E, B-3001 Leuven, Belgium. [3]Kenyatta University, Department of Zoological Sciences, PO Box 16778-80100, Mombasa, Kenya. [4]Geosciences Environnement Toulouse UMR 5563 & UR 234 IRD, Université Paul-Sabatier, Avenue Edouard Belin 14, F-31400 Toulouse, France. [5]Kenya Marine and Fisheries Research Institute, PO Box 81651, Mombasa-80100, Kenya. *e-mail: alberto.borges@ulg.ac.be
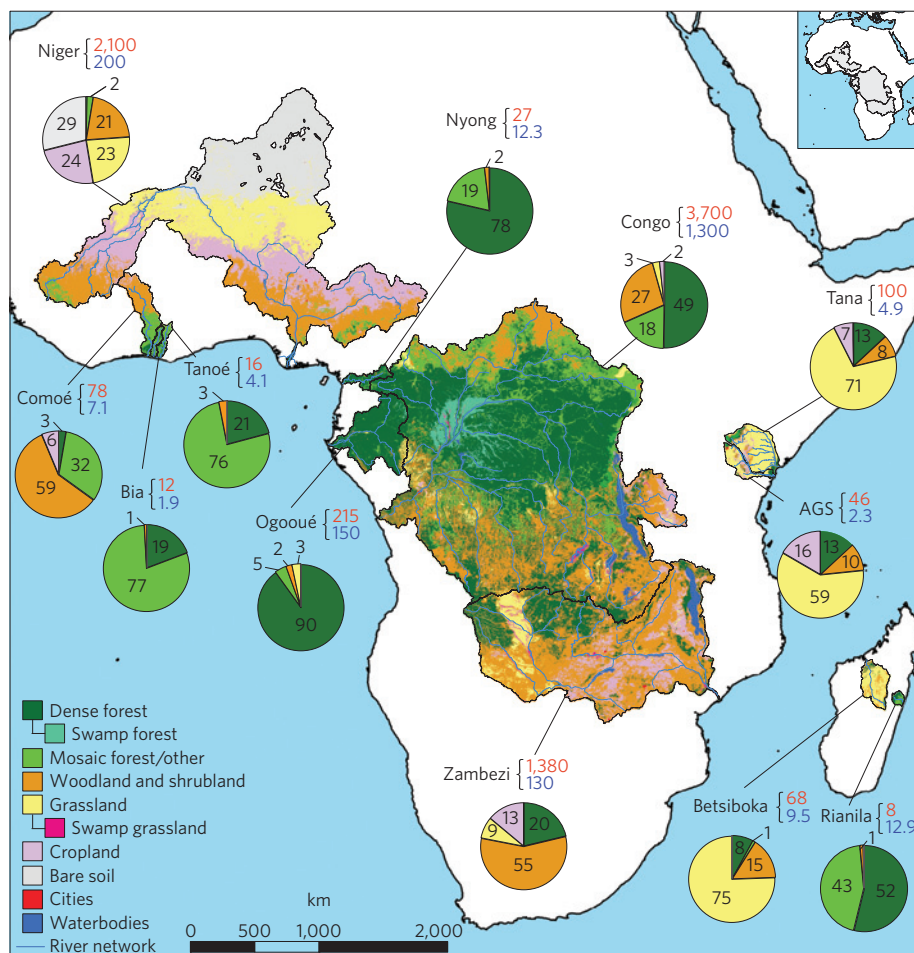
Figure 1 | The 12 studied rivers cover a wide range of discharge, catchment size and land cover. The red numbers correspond to the catchment surface area (10^3 km^2) and the blue numbers correspond to the annual freshwater discharge (km^3 yr^{-1}). Refer to Methods for data sources. AGS, Athi-Galana-Sabaki River.

(%O_2) (Supplementary Fig. 2). The overall average p_{CO_2} and CH_4 in rivers was 6,415 ppm and 2,205 nmol l^{-1}, respectively, corresponding to large over-saturation of surface waters with respect to atmospheric equilibrium of CO_2 and CH_4 (on average ~395 ppm and ~2 nmol l^{-1}, respectively). The N_2O values oscillated between under- and over-saturation, with an overall average of 9.2 nmol l^{-1}, only slightly above the atmospheric equilibrium of ~6.6 nmol l^{-1}.

The fluxes were computed from the gas transfer velocity (k) using two approaches. The Aufdenkampe *et al.* (Auf) approach[2] relies on constant k values across basins separated into streams and rivers (<100 m and >100 m width, respectively). The Raymond *et al.* (Ray) approach[3] uses basin-specific k values computed from hydraulic equations and basin characteristics. We present both estimates to provide a range of flux values, allowing a comparison with published fluxes. An error analysis is provided in the Supplementary Methods and Methods. Among river systems, the air–water CO_2 fluxes computed with the Auf approach (FCO_{2Auf}) ranged between 186 ± 9 and $1,149 \pm 53$ mmol m^{-2} d^{-1}, the air–water CH_4 fluxes (FCH_{4Auf}) ranged between 0.5 ± 0.1 and 18 ± 1 mmol m^{-2} d^{-1}, and the air–water N_2O fluxes (FN_2O_{Auf}) ranged between 2.0 ± 0.1 and 16 ± 1 µmol m^{-2} d^{-1} (Supplementary Table 3). The fluxes computed using the Ray approach were ~1.34 times higher, as it accounts for lower-order streams that are more turbulent and have higher k values. The average FCO_2 for all rivers was 11 times higher than FCH_4 (in CO_2e) and 273 times higher than FN_2O (in CO_2e). For individual basins, the FCO_2:FCH_4 ratio

ranged between 4 (Zambezi) and 39 (Tana). This is in contrast to other concurrent FCO_2, FCH_4 and FN_2O estimates in temperate rivers (Supplementary Table 4), where FCO_2:FCH_4 ratios are higher (between 9 and 411, average 108) and FCO_2:FN_2O ratios are lower (between 10 and 71, average 35). This reflects the less extensive flooded areas in these temperate rivers (floodplains promote FCH_4 compared to FCO_2), and higher inputs of fertilizer- or wastewater-derived nitrogen, which promote FN_2O (ref. 5) compared to FCO_2.

The FCO_{2Ray} we report were 1.1–4.7 times (on average 2.6 times) higher than those given by Raymond *et al.*[3] for the same basins (Supplementary Fig. 3), suggesting that the reliance of the latter on a very limited African p_{CO_2} database resulted in underestimating the riverine FCO_2 for the African continent. When comparing the surface-area-integrated FCO_2 per basin (Supplementary Table 3) to the flux of total organic C (TOC) and dissolved inorganic C (DIC) to the ocean for the Congo, the Zambezi and the Tana (data are unavailable for other rivers sampled), FCO_2 was, respectively, 8.6, 2.1 and 9.9 times higher than the TOC+DIC export to the ocean, or 13.3, 16.5 and 23.0 times higher than the TOC export to the ocean. By comparison, in the Amazon River, the total FCO_2 is 6.6 and 13.1 times higher than the TOC+DIC and TOC export to the ocean[14]. This clearly highlights the significance of vertical C fluxes from inland waters to the atmosphere.

Regional and global significance of GHG fluxes

The FCO_2 integrated for all SSA rivers ranged between 0.27 ± 0.05 (Auf) and 0.37 ± 0.07 (Ray) PgC yr^{-1}. Such values are of the same
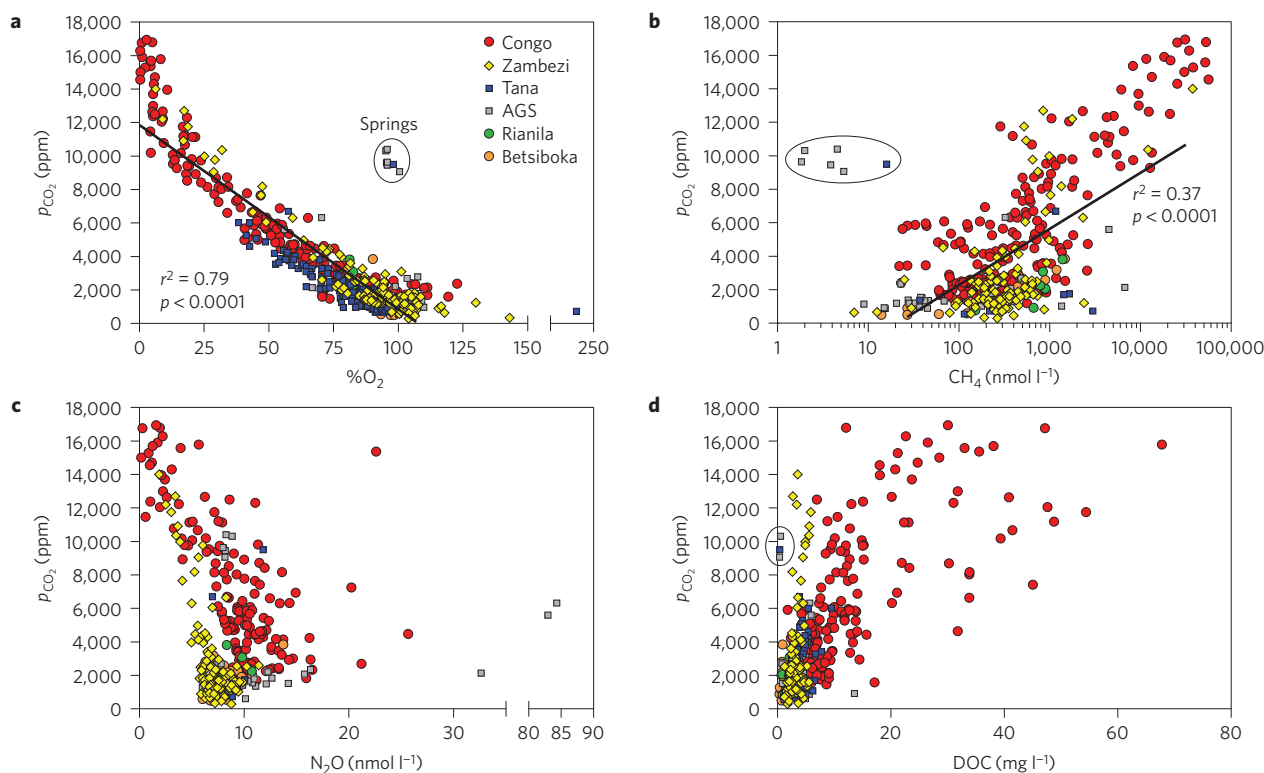
Figure 2 | Complex interplay of biogeochemical processes is revealed by GHGs property–property relations. p_{CO_2} as functions of $\%O_2$ (**a**), log CH_4 (**b**), N_2O (**c**) and DOC (**d**) in six African river systems. The encircled data points correspond to water from springs that are enriched in CO_2, depleted in CH_4 and DOC owing to bacterial removal in groundwaters and at O_2 saturation owing to rapid equilibration with the atmosphere. Lines correspond to a linear regression fit.

order of magnitude as the integrated FCO_2 for the Amazon River of 0.47 PgC yr⁻¹ (ref. 14), although the latter estimate included wetlands that accounted for 86% of flooded land whereas river channels only occupied 14% (ref. 13). The FCH_4 integrated for all rivers in SSA ranged between 2.9 ± 0.1 (Auf) and 3.9 ± 0.1 (Ray) TgC yr⁻¹. This is roughly five times higher than the FCH_4 recently attributed for all tropical rivers (0.7 TgC yr⁻¹) in a recent data synthesis[4], where, in the absence of empirical data from the tropics, the average CH_4 flux from temperate rivers was upscaled. The sum of integrated FCO_2 and FCH_4 ranged between 0.29 ± 0.05 (Auf) and 0.39 ± 0.07 (Ray) $PgCO_2e$ yr⁻¹. These values are highly significant when compared to other fluxes at the scale of the African continent given by the most recent overarching synthesis[8], such as the C emission from fossil fuel (∼1.25 PgC yr⁻¹), terrestrial net ecosystem production (NEP) (1.2–2.9 PgC yr⁻¹), or TOC+DIC export to the ocean (0.06 PgC yr⁻¹). The emission of CO_2 and CH_4 in CO_2e from SSA rivers would thus balance two-thirds of the reported net C sink for continental Africa (0.6 ± 0.6 PgC yr⁻¹; ref. 8). Note that the net C sink estimate of the latter did not account for the fluxes from inland waters.

We propose that our emission estimates of CO_2 and CH_4 from SSA rivers may be conservative for two reasons. First, the FCH_4 values correspond only to diffusive emissions and do not account for CH_4 ebullition, which can be highly significant in tropical aquatic environments[17–19]. Based on floating chamber flux measurements in the Congo and Zambezi rivers ($n = 68$), we found CH_4 ebullition rates to be on average 0.25 times the diffusive CH_4 flux (Supplementary Fig. 4). This compares well with data from six Amazon river channels, where CH_4 ebullition was 0.33 times the diffusive CH_4 flux[19]. Applying a factor of 0.25 to estimate the CH_4 ebullition, the sum of integrated FCO_2 and FCH_4 would then range between 0.30 ± 0.05 (Auf) and 0.40 ± 0.07 (Ray)

$PgCO_2e$ yr⁻¹. Second, our estimates do not account for extensive tropical wetlands, which in the Amazon are known to show CH_4 fluxes two orders of magnitude higher than river channels[17]. The Congolese 'Cuvette Centrale', with a flooded surface area of 360×10^3 km² (ref. 20), is the second largest tropical wetland area after the Amazon. The sum of FCO_2 and FCH_4 from the 'Cuvette Centrale' would correspond to 0.48 ± 0.08 $PgCO_2e$ yr⁻¹ (based on the scaling of a subset of fluxes from the rivers, streams and navigation channels draining the 'Cuvette Centrale' and computed with the k recommended for flooded areas[2]). The above FCH_4 estimate for the 'Cuvette Centrale' does not include the ebullition of CH_4; using a reported ebullition:diffusion ratio of 0.73 for tropical wetlands[18] would bring the total FCO_2 and FCH_4 from SSA rivers and wetlands to range between 0.85 ± 0.10 (Auf) and 0.95 ± 0.11 (Ray) $PgCO_2e$ yr⁻¹. These fluxes are significant beyond the African continental scale, considering that the global net CO_2 sink is at present estimated at 1.5 and 2.0 PgC yr⁻¹ for the oceans and the terrestrial biosphere, respectively[7].

Processes underlying GHG dynamics

Although it is crucial to quantify GHG fluxes, unravelling the underlying processes is equally important. This can be attempted with a correlation analysis with other biogeochemical variables and catchment characteristics. The p_{CO_2} data were well correlated to $\%O_2$ and to the log of CH_4 (Fig. 2a,b), suggesting that the dynamics of the three variables were driven by net heterotrophy[1]. The lowest N_2O values (below atmospheric equilibrium) were observed at the highest p_{CO_2} (Fig. 2c) and lowest $\%O_2$ levels (Supplementary Fig. 5), suggesting the removal of N_2O by denitrification, as also reported in the Amazon floodplains[21]. No distinct relationship could be established between N_2O and either nitrate (NO_3^-), ammonium (NH_4^+), or dissolved inorganic nitrogen ($DIN = NO_3^- + NH_4^+$)
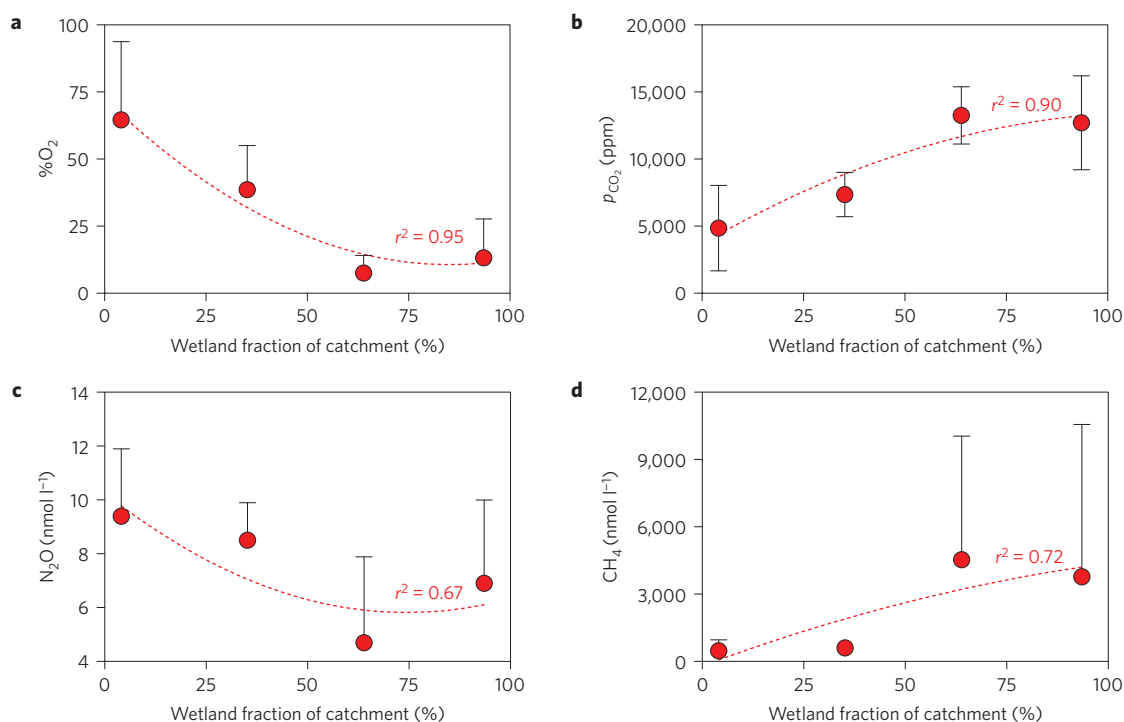
Figure 3 | Wetland presence drives the pattern of GHGs and O$_2$ in the Congo River. %O$_2$ (**a**), p_{CO_2} (**b**), N$_2$O (**c**) and CH$_4$ (**d**) in 46 rivers of the Congo basin as a function of wetland fraction of catchment surface. Data were bin-averaged in intervals of 25%. Two extreme CH$_4$ values (>25,000 nmol l^{-1}) were removed from the analysis. Error bars show mean ± s.d. Lines correspond to a second-degree polynomial fit.

(Supplementary Fig. 5), unlike in some temperate rivers[5]. In three of the sampled rivers, data sets from long-term fixed station monitoring showed a positive relationship between N$_2$O and NO$_3^-$ (Supplementary Fig. 6). The sampled rivers had relatively low DIN values[22], as fertilizer use is minimal within the catchments studied[23], and samples were not directly impacted by wastewaters from major cities; the only exception being the upper reaches of the Athi River, which are strongly influenced by wastewater inputs from Nairobi[22] and where the highest N$_2$O concentrations were recorded (Supplementary Fig. 3).

No relationship could be established between GHGs and elevation or water temperature (Supplementary Fig. 7). There was a general positive relationship between p_{CO_2} and dissolved organic C (DOC) (Fig. 2d) that has been used to infer the role of terrestrial organic matter inputs in sustaining net heterotrophy and CO$_2$ production within inland waters[9], although this can also be interpreted as an indication of concurrent DOC and CO$_2$ inputs from soils or wetlands. The p_{CO_2} in the Congo River levelled off for DOC concentrations >15 mg l^{-1}, which may indicate a limitation of bacterial growth (and subsequent CO$_2$ production) by the low pH in these very acidic organic environments (so called 'black waters', with pH between 3.6 and 5.9 and averaged 4.4), O$_2$ availability (%O$_2$ ranged between 0.3% and 93.5% and averaged 23.4%; Supplementary Fig. 8), or phosphorus availability as reported in other tropical black water rivers[24].

Concentrations of GHGs increased as the wetland fraction of the catchment surface increased for individual catchments (Congo River) and across river systems (Figs 3 and 4). In the Congo River, p_{CO_2} and CH$_4$ were positively related to wetland fraction, whereas %O$_2$ and N$_2$O were negatively related to the latter (Fig. 3). The CO$_2$, CH$_4$ and %O$_2$ patterns in the Congo tributaries along a 1,700 km river stretch (Supplementary Fig. 9) and in the Zambezi River[25] also follow the presence of wetlands. Similarly, a relationship between CH$_4$, p_{CO_2} and %O$_2$ with wetland fraction was also found across river systems (Fig. 4), consistent with findings in the Amazon basin,

where CO$_2$ emissions from wetland lakes and river channels have been attributed to organic C from wetlands[11–13] that also sustain intense CH$_4$ evasion[17].

However, basins that are virtually devoid of wetlands, such as the Tana (<0.5% of the catchment), were also found to be sources of CO$_2$, although admittedly lower than other SSA rivers. This suggests that part of the CO$_2$ emissions from SSA rivers are partly sustained by upland biomass. The increase of CO$_2$ and CH$_4$ and decrease of %O$_2$ in the Congo tributaries also follow the downstream increase of aboveground biomass and of the relative dense forest cover (Supplementary Figs 9 and 10). These patterns were also observed across river systems, although the Rianila catchment deviated from the general pattern owing to much steeper slopes within the basin (Supplementary Fig. 11). This highlights the role of relief, whereby gentle slopes increase water residence time and the extent of flooded areas, and steeper slopes enhance k, which drives dissolved GHG concentrations closer to saturation[26]. Precipitation has been previously used to model river CO$_2$ regionally[26]. We indeed found a positive relationship between p_{CO_2} and CH$_4$ and precipitation across SSA rivers, with the exception of the two Malagasy rivers (Supplementary Fig. 11). For the Rianila, this might also be related to the steeper slope. In the Betsiboka, nearly all of the yearly precipitation occurs from December to March, the rest of the year being extremely dry, leading to vegetation typical of a semi-arid climate. This suggests that models to predict p_{CO_2} from precipitation should also account for the regional differences in seasonal patterns.

Lateral inputs versus *in situ* respiration as CO$_2$ drivers

In addition to our GHG concentration measurements, we acquired 812 aquatic community respiration (*R*) data (Supplementary Fig. 12). The *R* values ranged between 0.3 and 404.0 mmolC m^{-3} d^{-1}, with a median of 20.0 mmolC m^{-3} d^{-1}, which is close to the median value of pelagic bacterial respiration reported in a recent data synthesis in tropical inland waters[27]. On individual paired mea-
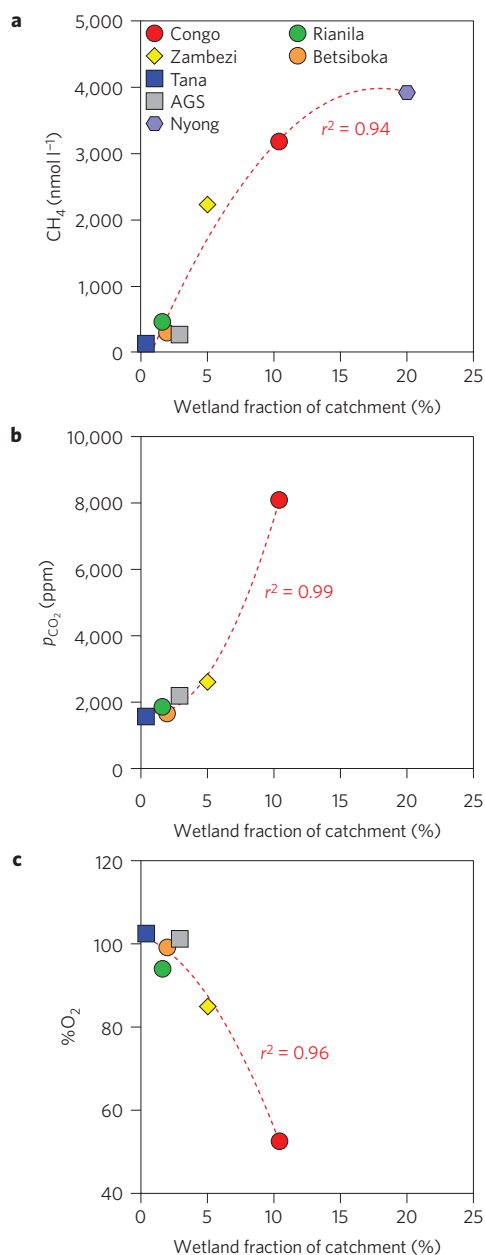
Figure 4 | Wetland presence drives the pattern of CO_2 and CH_4 concentrations across sub-Saharan African Rivers. p_{CO_2} (**a**), CH_4 (**b**) and $\%O_2$ (**c**), as a function of the wetland fraction of catchment surface (%) in seven African rivers. Only the data sets that capture spatial variations were included in the analysis (excluding fixed time series in the mainstem of rivers). Lines correspond to a second-degree polynomial fit.

surements, the FCO_2 was on average 8 times (Auf) to 12 times (Ray) higher than vertically integrated R ($n = 602$). The median R was 99.4 mmolC m^{-2} d^{-1}, which, when upscaled to all SSA rivers, can account only for 11% of the FCO_2 (0.27 PgC yr^{-1}). Although benthic respiration was not measured during our study, using the average value from a recent data synthesis for tropical rivers and streams (50.8 mmolC m^{-2} d^{-1}; ref. 28), we find that pelagic and benthic R combined still account for only <14% of the FCO_2. Furthermore, these estimates do not account for pelagic and benthic aquatic primary production, which would decrease the dissolved CO_2 concentration. These calculations imply that lateral inputs of CO_2 from soils, groundwaters and wetlands would be the largest contributors of the CO_2 emitted from rivers and streams.

Implications for understanding global C fluxes

Large CO_2 fluxes from inland waters have significant implications for our understanding of overall C fluxes and cycling at the landscape or catchment scale. The CO_2 emitted to the atmosphere from inland waters can be considered as a component of the respiration of upland and wetland vegetation, whether it is related to lateral transport of soil/wetland CO_2 (that is, respiration taking place in terrestrial or wetland habitats) or lateral transport of soil or wetland DOC and POC that is mineralized to CO_2 within the aquatic domain. Hence, the lateral transport of C from the upland terrestrial biosphere and wetlands to inland waters and its subsequent emission to the atmosphere offsets the estimates of terrestrial NEP. Furthermore, lateral transport of soil DOC leads to an underestimation of NEP based on biomass accumulation techniques, whereas the lateral transport of soil CO_2 leads to an overestimation of NEP derived from atmospheric measurements (eddy-covariance or flux towers). The significant FCO_2 from African inland waters at the continental scale is particularly important in the context of the mitigation of, and accounting for, GHG emissions, as C emissions related to tropical deforestation are only partially offset by C sequestration from forest regrowth[29]. Accounting for the additional C emissions from inland waters could further offset this balance. Alternatively, if most of the CO_2 emissions from SSA river channels are derived from wetland C, the net balance would be nearly neutral as it is balanced by the atmospheric CO_2 fixation by the emerged vegetation, as shown in the Amazon lowland areas[11–13]. Untangling the relative contributions of wetland and upland C in sustaining CO_2 and CH_4 emissions from inland waters is essential to better understand the role of tropical inland waters in the global C cycle and related potential feedbacks on a warming climate. Our results in SSA rivers show that this relative contribution is variable both within individual catchments and across catchments.

Methods

Methods and any associated references are available in the online version of the paper.

References

1. Cole, J. J. *et al.* Plumbing the global carbon cycle: Integrating inland waters into the terrestrial carbon budget. *Ecosystems* **10,** 171–184 (2007).
2. Aufdenkampe, A. K. *et al.* Riverine coupling of biogeochemical cycles between land, oceans, and atmosphere. *Front. Ecol. Environ.* **9,** 53–60 (2011).
3. Raymond, P. A. *et al.* Global carbon dioxide emissions from inland waters. *Nature* **503,** 355–359 (2013).
4. Bastviken, D., Tranvik, L. J., Downing, J. A., Crill, P. M. & Enrich-Prast, A. Freshwater methane emissions offset the continental carbon sink. *Science* **331,** 50 (2011).
5. Baulch, H. M., Schiff, S. L., Maranger, R. & Dillon, P. J. Nitrogen enrichment and the emission of nitrous oxide from streams. *Glob. Biogeochem. Cycles* **25,** GB4013 (2011).
6. IPCC *Climate Change 2013: The Physical Science Basis* (eds Stocker, T. F. *et al.*) (Cambridge Univ. Press, 2013).
7. Le Quéré, C. *et al.* Global carbon budget 2014. *Earth Syst. Sci. Data Discuss.* **7,** 521–610 (2014).
8. Valentini, R. *et al.* A full greenhouse gases budget of Africa: Synthesis, uncertainties, and vulnerabilities. *Biogeosciences* **11,** 381–407 (2014).
9. Lapierre, J.-F. & del Giorgio, P. A. Geographical and environmental drivers of regional differences in the lake p_{CO_2} versus DOC relationship across northern landscapes. *J. Geophys. Res.* **117,** G03015 (2012).
10. Maberly, S. C., Barker, P. A., Stott, A. W. & De Ville, M. M. Catchment productivity controls CO_2 emissions from lakes. *Nature Clim. Change* **3,** 391–394 (2013).
11. Melack, J. M. & Engle, D. L. An organic carbon budget for an Amazon floodplain lake. *Verh. Int. Verein. Limnol.* **30,** 1179–1182 (2009).

12. Engle, D. L., Melack, J. M., Doyle, R. D. & Fisher, T. R. High rates of net primary production and turnover of floating grasses on the Amazon floodplain: Implications for aquatic respiration and regional CO_2 flux. *Glob. Change Biol.* **14,** 369–381 (2008).

13. Abril, G. *et al.* Amazon River carbon dioxide outgassing fuelled by wetlands. *Nature* **505,** 395–398 (2014).

14. Richey, J. E., Melack, J. M., Aufdenkampe, A. K., Ballester, V. M. & Hess, L. Outgassing from Amazonian rivers and wetlands as a large tropical source of atmospheric CO_2. *Nature* **416,** 617–620 (2002).

15. Wang, Z. A. *et al.* Inorganic carbon speciation and fluxes in the Congo River. *Geophys. Res. Lett.* **40,** 511–516 (2013).

16. Abril, G. *et al.* Technical Note: Large overestimation of calculated p_{CO_2} in acidic, organic-rich freshwaters. *Biogeosciences* **12,** 67–78 (2015).

17. Melack, J. M. *et al.* Regionalization of methane emissions in the Amazon Basin with microwave remote sensing. *Glob. Change Biol.* **10,** 530–544 (2004).

18. Bastviken, D. *et al.* Methane emissions from Pantanal, South America, during the low water season: Toward more comprehensive sampling. *Environ. Sci. Technol.* **44,** 5450–5455 (2010).

19. Sawakuchi, H. O. *et al.* Methane emissions from Amazonian Rivers and their contribution to the global methane budget. *Glob. Change Biol.* **20,** 2829–2840 (2014).

20. Bwangoy, J.-R. B., Hansen, M. C., Roy, D. P., De Grandi, G. & Justice, C. O. Wetland mapping in the Congo Basin using optical and radar remotely sensed data and derived topographical indices. *Remote Sens. Environ.* **114,** 73–86 (2010).

21. Richey, J. E., Devol, A. H., Wofy, S. C., Victoria, R. & Riberio, M. N. G. Biogenic gases and the oxidation and reduction of carbon in Amazon River and floodplain waters. *Limnol. Oceanogr.* **33,** 551–561 (1988).

22. Marwick, T. R. *et al.* Dynamic seasonal nitrogen cycling in response to anthropogenic N loading in a tropical catchment, Athi–Galana–Sabaki River, Kenya. *Biogeosciences* **11,** 1–18 (2014).

23. Yasin, J. A., Kroeze, C. & Mayorga, E. Nutrients export by rivers to the coastal waters of Africa: Past and future trends. *Glob. Biogeochem. Cycles* **24,** GB0A07 (2010).

24. Castillo, M. M., Kling, G. W. & Allan, J. D. Bottom-up controls on bacterial production in tropical lowland rivers. *Limnol. Oceanogr.* **48,** 1466–1475 (2003).

25. Teodoru, C. *et al.* Spatial variability and temporal dynamics of greenhouse gas (CO_2, CH_4, N_2O) concentrations and fluxes along the Zambezi River mainstem and major tributaries. *Biogeosciences* **12,** 2431–2453 (2015).

26. Butman, D. & Raymond, P. A. Significant efflux of carbon dioxide from streams and rivers in the United States. *Nature Geosci.* **4,** 839–842 (2011).

27. Amado, A. M. *et al.* Tropical freshwater ecosystems have lower bacterial growth efficiency than temperate ones. *Front. Microbiol.* **4,** 167 (2014).

28. Cardoso, S. J., Enrich-Prast, A., Pace, M. L. & Roland, F. Do models of organic carbon mineralization extrapolate to warmer tropical sediments? *Limnol. Oceanogr.* **59,** 48–54 (2014).

29. Pan, Y. *et al.* A Large and persistent carbon sink in the World's forests. *Science* **333,** 988–993 (2011).

Author contributions

A.V.B. and S.B. conceived and designed the study and coordinated the project and fieldwork. Field data collection was carried out by all co-authors. T.L. carried out the geographical system information (GIS) analysis. A.V.B. drafted the manuscript, which was substantially commented upon and amended by S.B., C.R.T., T.R.M., N.G., T.L. and F.G. All co-authors approved the manuscript.

Additional information

Supplementary information is available in the online version of the paper. Reprints and permissions information is available online at www.nature.com/reprints. Correspondence and requests for materials should be addressed to A.V.B.

Competing financial interests

The authors declare no competing financial interests.

Methods

We acquired 1,880 data for CH_4, 1,625 data for N_2O and 693 data for p_{CO_2} from June 2006 to September 2014 in 12 river basins (Supplementary Table 1). The dissolved gases were measured with a uniform method based on the headspace technique, either directly in the field by infrared gas analysis (IRGA; for CO_2), or on return in the laboratory by gas chromatography (GC; for CH_4 and N_2O). Our analysis excludes p_{CO_2} data computed from pH and total alkalinity, because of strong biases due to the interference from organic acids, in particular in organic C rich black waters[15,16].

Sampling and field measurements. Two approaches were used during this study (Supplementary Table 1). First, a 'survey' approach aimed at sampling the mainstem of a river network over the longest possible stretch, as well as a maximum number of contributing tributaries, typically during a short period of time (2–60 d). In most cases, the surveys were done by car, with sampling from boats, bridges, or from the shore. In other cases, travel and sampling were carried out by boat (Congo River). Second, a 'monitoring' approach was applied at various fixed stations during a 1–2 yr period, with sampling taking place at monthly or fortnightly intervals in the mainstem of one or several rivers. The two approaches are highly complementary as the 'survey' approach provides a snapshot of the spatial variability, whereas the 'monitoring' approach provides the range of seasonal variability, but with little or no description of the spatial heterogeneity.

Water was collected with a Niskin bottle just below the surface (<0.5 m) and two serum bottles (50 ml) for the determination of CH_4 and N_2O were filled through tubing, allowed to overflow, poisoned with a saturated solution of $HgCl_2$ (50–100 µl), sealed with butyl stoppers, crimped with aluminium caps, and stored at ambient temperature in the dark. Samples for the determination of p_{CO_2} were directly collected in surface waters in four plastic 60 ml syringes and 30 ml of sample water was equilibrated with 30 ml of ambient air (5–10 min of vigorous shaking). The p_{CO_2} in ambient air and in the equilibrated gas phase were determined with a portable IRGA, from which the *in situ* p_{CO_2} was computed using the temperature values *in situ* and in the equilibrated water (that is, in the syringe), and Henry's constant. The IRGAs were calibrated with N_2 and a CO_2:N_2 commercial mixture (Air Liquide Belgium) with a mixing ratio of 1,017 ppm of CO_2 (PP Systems EGM-4 and Li-Cor Li-820) or with N_2 and a suite of CO_2:N_2 commercial mixtures (Air Liquide Belgium) with mixing ratios of 388, 813, 3,788 and 8,300 ppm CO_2 (Li-Cor Li-840). The Li-840 was used on the Congo in December 2013 and June 2014, the EGM-4 was used on the Congo in December 2012 and September 2013 and on the Zambezi, whereas the Li-820 was used on the Malagasy, Tana and Athi-Galana-Sabaki rivers. In the Congo in March 2013, the headspace was injected in pre-evacuated 12 ml Exetainer (Labco) vials and the CO_2 content was analysed by GC back in the laboratory (see hereafter). The overall precision of p_{CO_2} measurements was ±2.0% ($n = 447$ replications of three to four measurements).

Water temperature, conductivity, %O_2 and pH were measured *in situ* with portable field probes calibrated using standard protocols (in most cases using an YSI Proplus probe). Pelagic R was determined from the decrease of O_2 in 60 ml biological oxygen demand bottles over ~24 h incubation periods. The bottles were kept in the dark and close to *in situ* temperature in a cool box filled with *in situ* water. The O_2 decrease was determined from triplicate measurements at the start and the end of the incubation with an optical O_2 probe (YSI ProODO), and R data were converted into carbon units using a respiratory quotient of 1.3 (ref. 30). Samples for the DOC determination were preserved in 40 ml borosilicate vials with polytetrafluoroethylene-coated stoppers and preserved with H_3PO_4 (85%) after filtration through 0.2 µm pore size polyethersulphone (PES) syringe filters. Samples for nitrate (NO_3^-) and ammonium (NH_4^+) were filtered on a 0.2 µm PES syringe filter, collected in 50 ml plastic vials, to which was added 200 µl of H_2SO_4 5N.

Laboratory chemical analysis. Concentrations of CH_4 and N_2O were determined via the headspace equilibration technique (20 ml N_2 headspace in 50 ml serum bottles) and measured by GC (ref. 31) with a flame ionization detection (GC-FID) and electron capture detection (GC-ECD) with a SRI 8610C GC-FID-ECD calibrated with CH_4:CO_2:N_2O:N_2 mixtures (Air Liquide Belgium) of 1, 10 and 30 ppm CH_4 and of 0.2, 2.0 and 6.0 ppm N_2O, and using the solubility coefficients of CH_4 (ref. 32) and N_2O (ref. 33). For the Nyong, the CH_4 was determined with a SRI 8610C GC-FID calibrated with CH_4:N_2 mixtures (Air Liquide France) of 2, 10 and 100 ppm CH_4. For the Ivory Coast rivers, the CH_4 was determined by GC-FID, as described elsewhere[34]. The overall precision of measurements was ±3.9% ($n = 1,057$ duplicate measurements) and ±3.2% ($n = 900$ duplicate measurements) for CH_4 and N_2O, respectively. DOC was analysed according to either on a Thermo HiperTOC-isotope ratio mass spectrometer (IRMS) or with an Aurora1030 TOC analyser (OI Analytical) coupled to a Delta V Advantage IRMS, with a precision better than ±5% (ref. 35). NO_3^- and NH_4^+ concentrations were estimated by spectrophotometry, using the dichloroisocyanurate-salicylate-nitroprussiate colorimetric method for NH_4^+ (ref. 36) and the sulphanilamide colorimetric method for NO_3^- (refs 37,38). The detection limits were 0.30 and 0.15 µmol l^{-1} for NH_4^+ and NO_3^-, respectively.

GHG flux computations. The air–water gas flux (F) was computed according to

$$F = k\Delta C$$

where k is the gas transfer velocity and ΔC is the air–water gas concentration gradient[39], whereby a positive value corresponds by convention to an emission of gas from the water to the atmosphere.

We used the monthly average corresponding to time of sampling of atmospheric p_{CO_2} from Mount Kenya (Kenya, −0.05° N 37.80° E), retrieved from the GLOBALVIEW-CO2 database (Carbon Cycle Greenhouse Gases Group of the National Oceanic and Atmospheric Administration (NOAA), Earth System Research Laboratory (ESRL)) and of N_2O from Mauna Loa (Hawaii, 19.54° N–155.85° E) from the NOAA/ESRL Chromatograph for Atmospheric Trace Species (CATS) Program. For atmospheric CH_4, a constant mixing ratio of 1.9 ppm was used. Atmospheric mixing ratios were converted from dry air to wet air using the water vapour computed from temperature[33] and into corresponding dissolved concentrations using solubility coefficients of CO_2 (ref. 40), CH_4 (ref. 32) and N_2O (ref. 33). Fluxes of CH_4 and N_2O were converted into CO_2 equivalents based on the assumption that over a 100-year period the emissions of 1 kg of CH_4 and 1 kg of N_2O correspond to 34 kg and 298 kg of CO_2, respectively[6]. For k, we used two approaches. The first approach[2] uses a constant k normalized to a Schmidt number (Sc) of 600 (k_{600}) of 17.2 cm h^{-1} for streams and small rivers (<100 m width), of 12.3 cm h^{-1} for larger rivers (>100 m width) and of 2.4 cm h^{-1} for wetlands. The second approach[3] provides k_{600} values per river basin corresponding to the average value for the whole river network up to stream order 1 derived from hydraulic equations[41] and a geographical information system (GIS) description of corresponding input hydraulic variables for each catchment. The Sc numbers of CO_2, N_2O and CH_4 were computed from water temperature[42]. The F data were aggregated to derive one value per tributary and per river mainstem, before averaging for a given river system. The global F values were computed as averages weighted by water body surface area for each river catchment derived from the percentage of river/stream effective surface area per catchment given in ref. 3. The F values were similarly upscaled to SSA using the river/stream surface areas given in ref. 3.

FCO_2 and FCH_4 were measured in parallel with a floating chamber in 25 stations in the Congo basin, and 43 stations in the Zambezi basin. The floating chamber consisted of an opaque polyvinyl chloride cylinder 15 cm in height with a 38 cm internal diameter holding a volume of 17 l, and a 7-cm-long underwater skirt. The chamber was deployed for 30 min and the p_{CO_2} change inside the chamber was determined directly with an IRGA (30 s logging), whereas 30 ml gas samples for CH_4 extracted from inside the chamber at 0, 5, 10, 20 and 30 min interval were injected into 50 ml serum vials full of a hyper-saline solution (saturated solution of NaCl) for analysis in the laboratory by GC-FID. The fluxes were computed from the temporal change of the partial pressure of the gases, the law of perfect gases, and the geometry of the chamber[43]. The k_{600} of CO_2 was computed based on the measured FCO_2 and the p_{CO_2} in water and air. Assuming that the FCO_2 is exclusively diffusive (that is, that the CO_2 ebullition flux is negligible), this k_{600} of CO_2 allows the computation of the diffusive CH_4 flux from the dissolved CH_4 concentration. This in turn allows the computation of the ebullition CH_4 flux from the chamber CH_4 measurement that captures both ebullition and diffusive CH_4 fluxes. Chamber measurements have been assumed to provide biased k values[44], although often comparing satisfactorily with atmospheric flux measurements[45,46] or infrared imaging of the water surface[47]. The obtained average k_{600} in the Congo (12 ± 11 cm h^{-1}) was not significantly different from the average in the Zambezi (10 ± 11 cm h^{-1}) (unpaired t-test, $p < 0.05$). These values are distinctly lower than those computed by Raymond *et al.*[3] of 22 and 20 cm h^{-1} for the Congo and Zambezi, respectively. This is related to the fact that Raymond *et al.*[3] provide k_{600} values for the whole basin, including low-order streams that are more turbulent than higher-order streams and rivers, and characterized by higher k_{600} values[41]. Our data were acquired in the mainstem of rivers and adjacent large tributaries, typically high-order systems. The k_{600} values in the highest stream order in the Congo (9) and Zambezi (8) given by Raymond *et al.*[3] are, respectively, 14.5 and 13.3 cm h^{-1}—closer to those derived from our chamber measurements. The Congo and Zambezi streams (<100 m width) had k_{600} values (11 ± 10 cm h^{-1}) that were not significantly different from those (10 ± 7 cm h^{-1}) in rivers (>100 m width) (unpaired t-test, $p < 0.05$). These values were close to the k_{600} value for rivers (>100 m width) of 12 cm h^{-1}, but lower than the value for streams (<100 m width) of 17 cm h^{-1} given by Aufdenkampe and colleagues[2]. This reflects the fact that our data in the Congo and Zambezi were obtained in high-order streams, mainly in regions with gentle slopes (lowlands). Nevertheless, the actual accuracy of the chamber k values is irrelevant in the present case because we aimed at determining the CH_4 ebullition from the chamber measurements. Yet, these CH_4 ebullition estimates are probably conservative and provide underestimates, as for logistical reasons there was no replication of chambers and the deployment was short relative other studies, where it varies between 1 h (ref. 19) and 24 h (ref. 18). Indeed, CH_4 ebullition is notoriously heterogeneous both in space and time (across different timescales from

daily to seasonal)[48–51], and adequately capturing this heterogeneity would require a sampling effort and design incompatible with other aims of our research.

GHG flux error analysis. An error analysis on the GHG flux computation and upscaling was carried out by error propagation of the GHG concentration measurements, the k value estimates, and the estimate of surface areas of river channels to scale the areal fluxes, using a Monte Carlo simulation with 1,000 iterations. The uncertainty on the GHG concentrations led to an uncertainty of areal fluxes of $\pm 1.2\%$, $\pm 2.3\%$ and $\pm 5.2\%$ for CO_2, CH_4 and N_2O, respectively. Whereas no information is available in Aufdenkampe et al.[2] regarding the uncertainty on k values, the uncertainty on k given by Raymond et al.[3] was estimated to be $\pm 10.0\%$, based on the errors on slope and constant of the parameterization[41]. This leads to a cumulated uncertainty of areal fluxes of $\pm 4.6\%$, $\pm 4.9\%$ and $\pm 6.7\%$ for CO_2, CH_4 (diffusive) and N_2O, respectively. Ebullition of CH_4 is highly heterogeneous spatially and temporally[48–51], and it is difficult to quantify this uncertainty. We arbitrarily assigned an uncertainty of $\pm 50\%$ for CH_4 ebullition. This leads to a cumulated uncertainty of total areal fluxes of $\pm 29.4\%$ for CH_4 (diffusive + ebullitive). The river/stream surface areas reported by Raymond et al.[3] were estimated using two different hydraulic equations, which allow one to estimate an uncertainty of $\pm 31.0\%$. The overall uncertainty of integrated fluxes in river channels is $\pm 18.8\%$, $\pm 18.3\%$, $\pm 34.2\%$ and $\pm 19.2\%$ for CO_2, CH_4 (diffusive only), CH_4 (diffusive + ebullitive) and N_2O, respectively. The comparison of the wetland mapping of Bwangoy et al.[20] and of the Africover vegetation map, allows one to evaluate the uncertainty of the surface area of Congolese 'Cuvette Centrale' to $\pm 10\%$. The overall uncertainty of integrated fluxes in the Congolese 'Cuvette Centrale' is $\pm 7.0\%$ and $\pm 30.6\%$ for CO_2 and CH_4 (diffusive + ebullitive), respectively.

Other sources of uncertainty that are not straightforward to quantify relate to seasonal and spatial representativeness. For all spatial surveys, we paid particular attention to cover the widest possible spectrum of systems from mainstem to headwaters, to capture spatial variations in the most comprehensive way given logistical constraints. Data from all basins cover different hydrologic conditions and average fluxes capture seasonality. Spatial and seasonal variations have been presented and discussed for some basins in site-specific studies[22,25,34,52–54].

GIS analysis of catchment characteristics. Mean slope and drainage area were extracted from the HYDRO1K global hydrologic data set[55]. The fractional land cover type of the watershed was extracted from the Global Land Cover (GLC) 2000 database of Africa[56]. In total, 27 different land sub-classes are defined in the GLC database, taking into account the dominant vegetation class (namely trees, shrubs and grasses), phenology, seasonality, flooding regime and altitude. These sub-classes were aggregated in seven first-level classes based on vegetation structural categories: dense forest, mosaic forest/other, woodlands and shrublands, grasslands, agricultural lands, bare soils and others (water bodies, urban). Aboveground biomass in $Mg\,km^{-2}$ ($Mg = 10^9\,g$) was extracted from the Woods Hole Research Center (WHRC) pantropical national level C stock data set[57]. The extent of wetland and floodplain areas was extracted from the Global Lakes and Wetlands Database[58], except for the Nyong[59] and the Tana (Omengo, F. O. Based on A GIS Analysis of Landsat Images). Annual precipitation was extracted from the WorldClim Global Climate Database[60].

Data availability. The full data set of CO_2, CH_4 and N_2O concentrations is available as Supplementary Information.

Data sources. Several publicly available data sources were used:
HYDRO1K global hydrologic data set: https://lta.cr.usgs.gov/HYDRO1K
GLC 2000 database of Africa:
http://forobs.jrc.ec.europa.eu/products/glc2000/products.php
WHRC pantropical national level C stock data set:
http://www.whrc.org/mapping/pantropical/carbon_dataset.html
Global Lakes and Wetlands Database:
https://www.worldwildlife.org/pages/global-lakes-and-wetlands-database
WorldClim—Global Climate Data: http://www.worldclim.org
Data on river/stream surface and k values from: http://www.nature.com/nature/journal/v503/n7476/abs/nature12760.html#supplementary-information

References

30. Richardson, D. C., Newbold, J. D., Aufdenkampe, A. K., Taylor, P. G. & Kaplan, L. A. Measuring heterotrophic respiration rates of suspended particulate organic carbon from stream ecosystems. *Limnol. Oceanogr.* **11**, 247–261 (2013).
31. Weiss, R. F. Determinations of carbon dioxide and methane by dual catalyst flame ionization chromatography and nitrous oxide by electron capture chromatography. *J. Chromatogr. Sci.* **19**, 611–616 (1981).
32. Yamamoto, S., Alcauskas, J. B. & Crozier, T. E. Solubility of methane in distilled water and seawater. *J. Chem. Eng. Data* **21**, 78–80 (1976).
33. Weiss, R. F. & Price, B. A. Nitrous oxide solubility in water and seawater. *Mar. Chem.* **8**, 347–359 (1980).
34. Koné, Y. J. M., Abril, G., Delille, B. & Borges, A. V. Seasonal variability of methane in the rivers and lagoons of Ivory Coast (West Africa). *Biogeochemistry* **100**, 21–37 (2010).
35. Bouillon, S., Korntheuer, M., Baeyens, W. & Dehairs, F. A new automated setup for stable isotope analysis of dissolved organic carbon. *Limnol. Oceanogr.* **4**, 216–226 (2006).
36. Standing Committee of Analysts *Methods for the Examination of Waters and Associated Materials* (HMSO, 1981).
37. *Standard Methods for the Examination of Water and Wastewater* (APHA, 1998).
38. Miranda, K. M. et al. A rapid, simple spectrophotometric method for simultaneous detection of nitrate and nitrite. *Nitric Oxide* **5**, 62–71 (2001).
39. Liss, P. S. & Slater, P. G. Flux of gases across the air–sea interface. *Nature* **247**, 181–184 (1974).
40. Weiss, R. F. Carbon dioxide in water and seawater: The solubility of a non-ideal gas. *Mar. Chem.* **2**, 203–215 (1974).
41. Raymond, P. A. et al. Scaling the gas transfer velocity and hydraulic geometry in streams and small rivers. *Limnol. Oceanogr.* **2**, 41–53 (2012).
42. Wanninkhof, R. Relationship between wind speed and gas exchange over the ocean. *J. Geophys. Res.* **97**, 7373–7382 (1992).
43. Frankignoulle, M. Field measurements of air-sea CO_2 exchange. *Limnol. Oceanogr.* **33**, 313–322 (1988).
44. Raymond, P. A. & Cole, J. J. Gas exchange in rivers and estuaries: Choosing a gas transfer velocity. *Estuaries* **24**, 312–317 (2001).
45. Guérin, F. et al. Gas transfer velocities of CO_2 and CH_4 in a tropical reservoir and its river downstream. *J. Mar. Syst.* **66**, 161–172 (2007).
46. Huotari, J., Haapanala, S., Pumpanen, J., Vesala, T. & Ojala, A. Efficient gas exchange between a boreal river and the atmosphere. *Geophys. Res. Lett.* **40**, 5683–5686 (2013).
47. Gålfalk, M., Bastviken, D., Fredriksson, S. & Arneborg, L. Determination of the piston velocity for water–air interfaces using flux chambers, acoustic Doppler velocimetry, and IR imaging of the water surface. *J. Geophys. Res.* **118**, 770–782 (2013).
48. Crawford, J. T. et al. Ebullitive methane emissions from oxygenated wetland streams. *Glob. Change Biol.* **20**, 3408–3422 (2014).
49. DelSontro, T. et al. Spatial Heterogeneity of methane ebullition in a large tropical reservoir. *Environ. Sci. Technol.* **45**, 9866–9873 (2011).
50. Deshmukh, C. et al. Physical controls on CH_4 emissions from a newly flooded subtropical freshwater hydroelectric reservoir: Nam Theun 2. *Biogeosciences* **11**, 4251–4269 (2014).
51. Maeck, A., Hofmann, H. & Lorke, A. Pumping methane out of aquatic sediments – ebullition forcing mechanisms in an impounded river. *Biogeosciences* **11**, 2925–2938 (2014).
52. Bouillon, S. et al. Organic matter sources, fluxes and greenhouse gas exchange in the Oubangui River (Congo River basin). *Biogeosciences* **9**, 2045–2062 (2012).
53. Bouillon, S. et al. Contrasting biogeochemical characteristics of right-bank tributaries and a comparison with the mainstem Oubangui River, Central African Republic (Congo River basin). *Sci. Rep.* **4**, 5402 (2014).
54. Bouillon, S. et al. Distribution, origin and cycling of carbon in the Tana River (Kenya): A dry season basin-scale survey from headwaters to the delta. *Biogeosciences* **6**, 2475–2493 (2009).
55. *HYDRO1K Elevation Derivative Database* (US Geological Survey, 2000).
56. Mayaux, P., Bartholomé, E., Fritz, S. & Belward, A. A new land-cover map of Africa for the year 2000. *J. Biogeogr.* **31**, 861–877 (2004).
57. Baccini, A., Laporte, N., Goetz, S. J., Sun, M. & Dong, H. A first Map of tropical Africa's above-ground biomass derived from satellite imagery. *Environ. Res. Lett.* **3**, 045011 (2008).
58. Lehner, B. & Döll, P. Development and validation of a global database of lakes, reservoirs and wetlands. *J. Hydrol.* **296**, 1–22 (2004).
59. Olivry, J. C. *Fleuves et Rivières du Cameroun* (MESCES – ORSTOM, 1986).
60. Hijmans, R. J., Cameron, S. E., Parra, J. L., Jones, P. G. & Jarvis, A. Very high resolution interpolated climate surfaces for global land areas. *Int. J. Clim.* **25**, 1965–1978 (2005).